Thermo-mechanical characterization of surface-micromachined microheaters using in-line digital holography

Jayaraman, Balaji; Singh, Vijay Raj; Anand, Asundi; Bhat, Navakanta; Hegde, Gopalkrishna M.

2010

Jayaraman, B., Singh, V. R., Anand, A., Bhat, N., & Hegde, G. M. (2010). Thermo-mechanical characterization of surface-micromachined microheaters using in-line digital holography. Measurement Science and Technology, 21(1).

https://hdl.handle.net/10356/94023

https://doi.org/10.1088/0957-0233/21/1/015301

Thermo-mechanical characterization of surface-micromachined microheaters using in-line digital holography

Balaji Jayaraman[1], Vijay Raj Singh[2], Anand Asundi[2], Navakanta Bhat[1] and Gopalkrishna M Hegde[3]

[1] Department of Electrical Communication Engineering and Centre of Excellence in Nanoelectronics, Indian Institute of Science, Bangalore-560012, India

[2] School of Mechanical and Aerospace Engineering, Nanyang Technological University, Singapore-639798, Singapore

[3] Department of Aerospace Engineering, Indian Institute of Science, Bangalore-560012, India

E-mail: navakant@ece.iisc.ernet.in and hegopal@aero.iisc.ernet.in

ABSTRACT

This paper describes the application of lensless in-line digital holographic microscopy (DHM) to carry out thermo-mechanical characterization of microheaters fabricated through PolyMUMPs three-layer polysilicon surface micromachining process and subjected to a high thermal load. The mechanical deformation of the microheaters on the electrothermal excitation due to thermal stress is analyzed. The numerically reconstructed holographic images of the microheaters clearly indicate the regions under high stress. A double-exposure method has been used to obtain the quantitative measurements of the deformations, from the phase analysis of the hologram fringes. The measured deformations correlate well with the theoretical values predicted by a thermo-mechanical analytical model. The results show that lensless in-line DHM with Fourier analysis is an effective method for evaluating the thermo-mechanical characteristics of MEMS components.

Keywords

digital in-line holographic microscopy, lensless digital holography, double exposure, microheater, thermo-mechanical characterization.

1. INTRODUCTION

Microelectromechanical systems (MEMS) have become ubiquitous in sensor and actuator applications. They are used in varied fields working in multiple energy-domains such as thermal actuators, pressure sensors, accelerometers, RF switches and filters, etc. Dynamic characterization of MEMS devices forms an important part in carrying out their functional testing and reliability analysis. Microheaters are MEMS devices that possess significant advantages over conventional heaters such as small form factor, lower power consumption, uniform thermal distribution, lower thermal mass and enhanced isolation from the surroundings. The electrothermal excitation of the microheaters leads to

deformation of the device due to thermal stresses. This deformation could be characterized to obtain information on the uniformity of thermal stress distribution, and also on the reliability of the device. The MEMS structures are usually realized using different material layers, namely layers of polysilicon and metallic films encapsulated by silicon nitride and/or silicon dioxide, and involving various processing steps. In many applications, the microheaters are subjected to rapid and frequent temperature modulations. This, together with the temperature gradients along the structure, causes significant thermal stresses, which can adversely affect the lifetime of the device and even impact the device performance. These thermal stresses, which are induced during the operation of the microheater, provide a major contribution to the mechanical stress in the layers.

Various techniques have been explored for thermal characterization of MEMS devices. Thermographic techniques [1, 2] such as infra-red radiation analysis, fluorescent microthermographic imaging technique [3] and liquid crystal method [4] have been employed for thermal characterization of MEMS devices. These techniques possess limitations such as poor resolution, issues concerning repeatability or coating the device with different layers. Thermo-reflectometry, a non-destructive optical technique for thermal characterization, has been proposed [5]. Though the technique provides a spatial resolution of 0.5 μm to 1 μm, the main difficulty arises with the requirement of knowledge on a thermoreflectivity coefficient of the material used. The above-mentioned techniques are useful in estimating the device temperature. To characterize the deformations in the device, different sets of techniques have been adopted in the literature. A 3D surface profilometer involving the white light interferometric scanning principle with a stroboscopic LED light source, providing a vertical displacement resolution of 3–5 nm, has been proposed in [6]. In-plane motion characterization of MEMS resonators could be performed using a stroboscopic scanning electron microscope imaging technique [7]. The accuracy of the measured displacement using this technique is about 20 nm, limited mainly by the electron probe size and digital scanning resolution. Laser doppler vibrometry is also one of the widely used MEMS characterization techniques. Frequency response of vibration amplitude of the mechanical structures, along with their vibration modes, can be obtained using a vibrometer [8, 9], but it cannot provide the static deformation of the mechanical structures. Further, they provide vibration information at a single point. To analyze the vibrations of a device, the laser beam has to scan the entire structure.

To this end, use of digital holographic microscopy (DHM) in MEMS characterization has generated a lot of interest in recent years for the accurate determination of the deformations due to the residual stress and the impact of thermal loads on deformations. DHM provides a non-contact based and non-destructive method for the static as well as dynamic characterization of MEMS devices [10]. DHM has also been employed for the dynamic characterization of a bulk-micromachined microheater [11]. As this method uses lens geometry for hologram recording, the aberration introduced by the microscope objective has to be compensated and a focus-tracking procedure has to be followed before analyzing the digital holograms. In order to overcome these procedures a lensless in-line DH technique has been explored for various applications. In comparison to a well-

developed commercial off-axis set-up [12], the in-line system helps relax the spatial resolution requirement on the CCD sensor and increases the flexibility of the system. In-line geometry significantly improves the performance of a digital holography system and shows higher resolution and accuracy [13]. It is also shown that the in-line digital holographic system shows better performance due to its higher spatial-bandwidth product which provides a larger field of view and higher imaging resolution than the off-axis set-up [14]. Time-averaged in-line digital holography is used for the vibration characterization of MEMS diaphragms [15], wherein a double-exposure time-average technique is proposed to suppress the background noise due to in-line geometry as well as to separate the time-average vibration fringes and mean deformation fringes. The aim of this paper is to demonstrate the application of a lensless in-line DHM technique in thermo-mechanical characterization of surface-micromachined microheaters employing a double-exposure, time-average approach. The deformations due to thermal stress have been analyzed using a lensless DHM technique and an analytical model. The experimentally observed deformations are compared against the values obtained through a thermo-mechanical analytical model.

2. DEVICE FABRICAITON

Microheaters are basically resistive beams which can attain a temperature of 300–400 ◦C due to joule heating, when sufficient voltage is applied across them. The design of microheaters is optimized for low power consumption, low thermal mass, better temperature uniformity across the device and enhanced thermal isolation from the surroundings. The microheaters are fabricated through PolyMUMPs [16], a commercial three-layer polysilicon surface micromachining process used for MEMS applications. Polysilicon is the structural material and a phosphosilicate glass (PSG) is used as the sacrificial layer. The cross-sectional view of a generic device, depicting various layers in the PolyMUMPs process, is given in figure 1(*d*). A 0.6 μm Si_3N_4 film is deposited on an n-type silicon wafer. This is followed by a 0.5 μm polysilicon (poly-0) deposition. After patterning poly-0, 2 μm PSG is deposited. After patterning the PSG for anchors, 2 μm polysilicon (poly-1) is deposited, which forms the first structural layer. After patterning poly-1, 0.75 μm of PSG is deposited, and patterned to allow contacts to poly-1. This is followed by deposition and patterning of 1.5 μm polysilicon (poly-2), the second structural layer. The final step is the deposition of a 0.5 μm gold layer by evaporation. All the poly and PSG layers are deposited by LPCVD. The microheaters are realized on poly-1 and poly-2 layers. The poly-1 heaters have an air gap of 2 μm between the heater and the substrate and the poly-2 heaters have an air gap of 2.75 μm. Three different microheater structures are fabricated, namely double-meander (DM), double-spiral (DS) and serpentine (SERP), as shown in figure 1. The active area (the central area of the microheater wherein the temperature is the maximum) of the microheater is fixed at 140 μm × 140 μm in all three variants. In each variant, the length, width and spacing are varied to achieve different resistance values ranging from 200 Ω to 1850 Ω. The sheet resistances of poly-1 and poly-2 are 10 Ω/square and 20 Ω/square respectively. When the heaters are realized on poly-1, there is an additional poly-2 layer on top of the microheater. This is intended as an interdigitated electrode in a gas sensor application.

These electrodes make no contact to the microheater structure. Further, this interdigitated electrode structure is not present when the microheaters are realized on a poly-2 layer.

3. IN-LINE DHM-BASED CHARACTERISED METHOD

3.1. Optical system

The reflection lensless in-line DHM system geometry is shown in figure 2. The output from a He–Ne laser (632.8 nm) is coupled into a single mode fiber. The diverging output laser beam from the fiber end provides the magnification in a lensless geometry. The beam is divided into two parts by using a beam splitter: one beam illuminates the sample and the other is incident on the plane mirror. The scattered light from the sample (object beam) is combined with the other diverging beam, reflected from the mirror (reference beam) and the resulting interference pattern is recorded by the CCD.

The distance between the object and the CCD controls the magnification of the system. This set-up presents a lensless microscopic geometry by using a very simple and compact optical set-up best suited for micron-size objects. The effect of a zero-order term and twin image wave can be suppressed using a double-exposure method [15]. The polarization of the object and reference waves is maintained to get the best contrast of the interference fringes. The interference of object and reference beams, called a digital hologram, is recorded on the CCD at a frame rate of 30 frames/s. The CCD contains 1280 × 940 square pixels of 4.65 μm in size. The microheater is heated using a dc power supply. The in-line holograms are recorded at different voltages applied to the microheater and directly saved in the computer in real time.

3.2. Numerical reconstruction

The in-line hologram is the interference of an object wave with the in-line reference wave at the CCD plane (ξ, η), i.e.

$$\begin{aligned} H(m,n) &= |O(m,n) + R(m,n)|^2 \\ &= |O(m,n)|^2 + |R(m,n)|^2 \\ &\quad + O^*(m,n)R(m,n) + O(m,n)R^*(m,n). \end{aligned} \tag{1}$$

If the CCD contains $M \times N$ pixels with pixel size $\Delta\xi \times \Delta\eta$, then the digitally sampled hologram can be written as

$$\begin{aligned} H(m,n) &= \left[H(m,n) \otimes \operatorname{rect}\left(\frac{\xi}{\alpha \Delta\xi}, \frac{\eta}{\beta \Delta\eta} \right) \right] \\ &\quad \times \operatorname{rect}\left(\frac{\xi}{M\Delta\xi}, \frac{\eta}{N\Delta\eta} \right) \operatorname{comb}\left(\frac{\xi}{\Delta\xi}, \frac{\eta}{\Delta\eta} \right) \end{aligned} \tag{2}$$

where $\otimes$ represents the two-dimensional convolution and $(\alpha, \beta) \in [0, 1]$ are the fill factors of the CCD pixels.

The reconstruction of a hologram is a diffraction process. When the same reference wave is used to illuminate the hologram, the wavefield reconstructed at the distance d' at the image plane (x', y') is obtained as

$$U(x', y') = \frac{e^{ikd'}}{i\lambda d'} \int_{-\infty}^{\infty}\int_{-\infty}^{\infty} H(\xi, \eta) R(\xi, \eta) \times \exp\left[\frac{i\pi}{\lambda d'}\{(x' - \xi)^2 + (y' - \eta)^2\}\right] d\xi\, d\eta. \quad (3)$$

This equation can be converted into discrete form by using the parameters of the same CCD used for recording the holograms and can be written as the discrete Fresnel transformation [17]:

$$U(k, l) = \frac{e^{ikd'}}{i\lambda d'} e^{i\pi\lambda d'\left(\frac{k^2}{M^2\Delta\xi^2} + \frac{l^2}{N^2\Delta\eta^2}\right)} \sum_{k=0}^{M-1}\sum_{l=0}^{N-1} H(m, n) R(m, n) \times e^{\left[\frac{i\pi}{\lambda d'}(m^2\Delta\xi^2 + n^2\Delta\eta^2)\right]} e^{\left[-2\pi i\left(\frac{mk}{M} + \frac{nl}{N}\right)\right]} \quad (4)$$

where k =0,1,…,M-1,l=0,1,2,…,N-1.The matrix $U(k, l)$ is thus the discrete Fourier transformation of the product of hologram, $H(m, n)$the plane reference beam $H(m, n)$ and a phase term $exp\{i\pi/\lambda d'\}(m^2\Delta\xi^2 = n^2\Delta n^2)$ .The pixel size of the numerically reconstructed image varies with the reconstructed distance and is given by

$$\Delta x' = \frac{\lambda d'}{M\Delta\xi}, \qquad \Delta y' = \frac{\lambda d'}{N\Delta\eta}. \quad (5)$$

When the reconstruction distance d' equals the distance d between the object and the CCD during hologram recording, the real image of the object is formed at the image plane (x', y').

The amplitude and phase of the numerically reconstructed real image wave, apart from a magnification term, are as follows:

$$A(x', y') = |U(k, l)| \quad (6)$$

and

$$\phi(x', y') = \arctan\frac{\mathrm{Im}(U(k, l))}{\mathrm{Re}(U(k, l))}. \quad (7)$$

Because of in-line geometry, during reconstruction, the zero-order wave and the twin image overlap with this real image wave and thus provide the background noise. However, the use of a diverging wave, in an optical system, to illuminate the object reduces the noise of a twin image. It is because the twin image forms on the opposite side of a hologram plane to the real image and appears as a defocused image at the real image

plane. The effect of the zero-order wave and twin image is further suppressed using the double-exposure method.

3.3. Double-exposure method

In order to suppress these unwanted waves (background noise), the double-exposure method is used. In the double-exposure method, two in-line digital holograms corresponding to different deformation states of the object are recorded and then subtracted. The numerically reconstructed wave from the single hologram includes mainly two parts: one is the real image wave and the other is the background noise which is the sum of the zero-order wave and defocused twin image. Since the zero-order wave is the undiffracted reference wave and it does not change for the holograms recorded corresponding to the different deformation states of the object, the subtraction of the holograms completely removes the zero-order wave effect. As discussed before, the twin image wave diverges significantly at the real image plane; thus, the amplitude and phase of the twin image wave are considerably small in comparison to those of the real image wave. Hence, the subtraction of the reconstructed amplitude and phase information of the holograms at the real image plane suppresses the twin image effect and also provides information about the changes in the real image wave.

In this method, two in-line digital holograms of the object are recorded: one corresponding to the reference state (non-deformation), and the other is the deformed state. Consider an object having an out-of-plane deformation corresponding to the two states. The phase reconstructions of the holograms corresponding to these two states are called ϕ_1 and ϕ_2 respectively. The background noise at the real image plane due to zero-order and twin image waves does not change for different deformations of the same object except the variations in the stochastic speckle pattern between the two exposures. Hence, the subtraction of the amplitude and phase of the reconstructed wave suppresses the background noise. Subtraction of amplitudes directly provides the amplitude image changes during the double exposure of the object and subtraction of the phase directly provides the modulo 2π interference phase [18]. Figure 3 shows the flow chart of the reconstruction process for the double-exposure method.

4. THERMO-MECHANICAL ANALYSIS

In order to evaluate the temperature of an active area of the microheater, the temperature of the microheater was experimentally measured with the applied voltage [9]. The temperature coefficient of resistance α of the microheater is evaluated by placing the device on a thermal chuck and heating it to the required temperature. A small current (of the order of a few μA) is passed through the microheater to get the resistance values at different temperatures, and α is extracted from the slope of the resistance versus temperature plot, figure 4(*a*). The heater is then subjected to joule heating by applying a large voltage (of the order of a few volts) across the heater and the current is measured. The obtained resistance is mapped to the device temperature by using the α value. The calculated temperature would be an average value of the temperature across the entire device [19]. Figure 4(*b*) shows the temperature of one of the microheaters (SERP on

poly-1) as a function of the input electrical power. The effective thermal resistance is obtained from the slope of the curve as 2.49 $^{\circ}$C mW^{-1}. It is clear from the figure that the temperature of a microheater varies linearly with the input electrical power within the desired temperature range of the structure. Larger temperatures lead to increased thermal stresses on the heater structure, resulting in the mechanical deformation of the device. Also the repeated processing steps described previously can induce residual stress in the final structure of the microheater, which can appear in the form of undesired bowing of the resistive beam. The structural deformations arising due to thermal and residual stresses are analyzed using a lensless DHM technique which is non-contact based and non-destructive. In figure 5, a typical digital hologram of one of the microheaters (double-meandered structure, DM3 on poly-1 layer) is shown. The advantage of lensless DHM configuration is that a sequence of concentric circles that normally appear in the hologram as an effect of the phase distortion introduced by the microscope objective of the experimental set-up can be avoided. Otherwise, this aberration has to be removed first in order to obtain good reconstruction and accurate characterization of the system under test. The numerical reconstruction process is performed using equation (4) and simulated using MATLAB.

A thermo-mechanical model built to analyze the deformation of the microheater and electrode is discussed in the following subsection.

4.1. Thermo-mechanical model for a microheater–electrode system

Electrical power applied to the microheater results in heat generation in the heater. This leads to rise in heater temperature. This leads to rise in heater temperature. The top suspended electrode on a poly-2 layer also gets heated in the process due to convective heat transfer.

The electric power P applied to the microheater is given by

$$P = \frac{V^2}{R_H(1+\alpha_R \Delta T)} = \frac{V^2}{R_H(1+\alpha_R R_T P)} \qquad (8)$$

where α_R is the temperature coefficient of resistance, R_H is the electrical resistance of the microheater at room temperature, R_T is the thermal resistance of the microheater, V is the voltage applied across the heater.

Therefore,

$$P = \frac{-R_H + \sqrt{R_H^2 + 4\alpha_R R_T R_H V^2}}{2\alpha_R R_H R_T}. \qquad (9)$$

The microheater temperature for a given power is computed using the thermal resistance of the microheater:

$$T_H = P R_T + T_{\text{air}}. \qquad (10)$$

The temperature of the electrode is estimated by carrying out steady-state analysis of the thermal circuit of the microheater–electrode system.

Thermal resistances, R_c and R_{cv}, for conductive and convective heat transfers are given by

$$R_c = \frac{L}{kA}, \qquad R_{cv} = \frac{1}{hA} \qquad (11)$$

where L is the length over which the heat transfer takes place, k is the thermal conductivity of the material, A is the surface area of the element and h is the convective heat transfer coefficient. Heat losses due to radiation are ignored in this analysis as they are negligible for the temperature range of interest (<400 ◦C) [20] and for an air gap of 2 μm [21].

The thermal circuit of the microheater–electrode system in steady state is given in figure 6. Thermal gradient along the length of the microheater structure is not considered in this analysis. One-dimensional thermal analysis is done along the cross-section of the microheater at its center. Here q_g is the rate of heat generation in the microheater. q_{sub} represents the heat flow rate from the microheater to the substrate. q_{elec} represents the heat flow rate from the microheater to the top electrode with an overlap surface area of A_{H1} (2.315×10^{-9} m^2). q_{air} represents the heat flow rate from the microheater to the ambient from the rest of the surface area. Convective heat transfer occurs between the microheater and the electrode, and also between the electrode and the ambient. Within the electrode structure, there would be a temperature gradient along the cross-section due to thermal conduction. There would also be conductive heat transfer from the microheater to the substrate. As the temperature of the microheater is higher than that of the substrate, the conditions for fluid flow are stable, and hence there is no bulk fluid motion. Therefore, the heat transfer from the microheater to the substrate is by conduction, and not by free convection.

Since rate of heat flow along a branch in the network is constant, it follows that

$$q_{\text{elec}} = \frac{T_H - T_{\text{air}}}{\frac{1}{hA_{H1}} + \frac{L_3}{k_2 A_E} + \frac{1}{hA_E}} = \frac{T_H - T_{E\text{bot}}}{\frac{1}{hA_{H1}}} \qquad (12)$$

where A_E is the surface area of the top electrode (3.5×10^{-9} m^2), L_3 is the thickness of the top electrode (1.5 μm), $k2$ is the thermal conductivity of polysilicon (125 W m^{-1} K^{-1}),

h is the convective heat transfer coefficient for air (5 W m^{-2} K^{-1}) and T_{air} is the ambient temperature (25 ◦C).

Therefore, the temperature T_{Ebot} at the bottom surface of the electrode is given by

$$T_{Ebot} = T_H - \frac{1}{hA_{H1}} \left(\frac{T_H - T_{air}}{\frac{1}{hA_{H1}} + \frac{L_3}{k_2 A_E} + \frac{1}{hA_E}} \right). \qquad (13)$$

Similarly, the temperature T_{Etop} at the top surface of the electrode is given by

$$T_{Etop} = T_{Ebot} - \frac{L_3}{k_2 A_E} \left(\frac{T_H - T_{Ebot}}{\frac{1}{hA_{H1}}} \right). \qquad (14)$$

The average temperature of the electrode is given by

$$T_E = \frac{T_{Ebot} + T_{Etop}}{2}. \qquad (15)$$

Estimated temperatures of the microheater and the top electrode, with varying power, are shown in figure 7. As observed from the figure, there is a significant temperature rise in the top electrode as well due to convective heat transfer from the microheater, even though they are not electrically connected.

In order to calculate the thermal stress-induced deflections in the microheater and the electrode, the top electrode is approximated to a simple cantilever beam of length L (270 μm), and the microheater is approximated to a doubly clamped beam of length L_H (837.5 μm). Considering appropriate boundary conditions, the transverse displacement of the cantilever beam along its length is given by

$$u(x) = \frac{F_T x^2}{24 E_e I_e L}(x^2 - 4Lx + 6L^2) \qquad (16)$$

where F_T /L is the equivalent uniformly distributed load acting on the beam due to thermal stress, $I_e = \frac{\omega_e t_e^3}{12}$ is the area moment of inertia, E_e is Young's modulus of elasticity the electrode element. ω_e (10 μm) and t_e (1.5 μm) are the width and thickness of the cantilever beam. F_T is proportional to the thermal stress, and is given by

$$F_T = P_c \alpha_E \, (T_E - T_{\text{air}}) \, E_e \qquad (17)$$

where α_E is the coefficient of thermal expansion for polysilicon and P_c is a proportionality constant. The transverse displacement of the doubly clamped beam along its length is given by

$$u_H(x) = \frac{F_{TH} x^2 (x - L_h)^2}{24 E_h I_h L_h} \qquad (18)$$

where $F_{TH} = P_c \alpha_E \, (T_H - T_{\text{air}}) E_h$, L_h is the length of the doubly clamped beam, $I_e = \frac{\omega_h t_h^3}{12}$ is the area moment of inertia, E_h is Young's modulus of elasticity for polysilicon, ω_h (35μm) is the width of the microheater and t_h (2 μm) is the thickness of the microheater layer.

4.2. Thermal deformation characterization using DHM

Digital holographic characterization is performed on a double-meandered structure microheater (DM3-P1). Numerically reconstructed amplitude images of the DM3-P1 microheater at different applied voltages are shown in figure 8. These images are obtained without aberration correction and focus tracking. The main advantage of the DHM technique is that a quantitative evaluation of the deformation experienced by the heater membrane can be obtained from the phase analysis of a digital hologram. For thermal deformation analysis, the numerical phase reconstruction of the hologram is performed. Holograms were recorded at each voltage varying from 1 V to 10 V. The phase information is reconstructed corresponding to each state. The subtraction of the phases of the deformed state (corresponding to the applied voltage) and reference state (without applying voltage) provides the deformation fringes. Figures 8(*a*)–(*l*) clearly show the deformation fringes on the microheater for the applied voltages from 1.0 V to 3.75 V. As expected, the number of fringes increases with an increase in the applied voltage which clearly shows the increase in thermal deformation at higher temperatures. However, the observed change in the fringe pattern is not rapid confirming the lesser deformation of the microheater at lower temperatures.

The deformation fringes corresponding to the higher voltages (7.0–9.75 V) are shown in figures 9(*a*)–(*l*). The number of fringes on the microheater is large which shows the larger thermal deformation. It can also be observed that the deformation fringes are expanded on the electrodes that are above the microheater structure, and this increases with increase in temperature. This is due to the thermal expansion of both the microheater and the electrode during the high temperature operation of the microheater. The figure shows the full field thermal deformation in the device at higher temperatures. Thus, this kind of analysis is particularly useful for the full field study of micro-devices, where different components of the device show different deformation behavior, subject to the same input conditions. Since the reconstruction is done normal to the heater surface, the deformation fringes show the phase map for out-of-plane deformations.

The structural deformation due to thermal stress is quantitatively obtained from the phase analysis of hologram fringes. The vertical deformation is measured at two points: one on the electrode, and the other on the microheater, as indicated in figure 5(b). The amplitude of deformation at the applied voltage can be calculated from the obtained fringe patterns shown in figures 8 and 9. To do this, the phase difference value is converted into the path difference which represents the vertical deformation. Since an 8 bit CCD sensor is used for recording the hologram and the wavelength of a source is 632.8 nm, it provides a theoretical vertical measurement accuracy of about 2.5 nm. The experimentally obtained deformations for the microheater and the electrode, as a function of applied power, are compared with the analytically calculated deflections of the doubly clamped beam (at the center of the beam) and cantilever beam (at a distance of 0.8 L from the fixed end) in figure 10. It is observed that the analytically obtained values closely match the experimentally observed deformations. As the electrode has a much lower spring constant (0.249 N m^{-1}) compared to the microheater structure (2.44 N m^{-1}), the vertical deflection of the electrode is much higher than the microheater.

The proposed analysis is very useful in studying the response of different parts of the same micro-device simultaneously, for the same input conditions, and the method can be applied to characterize the MEMS structures. Thus, the thermo-mechanical characterization of MEMS-based microdevices using a lensless in-line DHM technique is useful in inferring the residual stress inside the structure. Analysis of a deformation profile under operating conditions using a nondestructive approach is useful in evaluating the effect of a heating cycle on the structure and the effect of a fabrication process on the final behavior of the microheater in order to ensure a reliable fabrication of the microheater. The proposed method can also be extended to measurement of non-periodic deformation. In particular, applying this method of characterization, it is possible to evaluate the deformation profile of the MEMS structures not only under the static condition but also under the dynamic condition by taking a sequence of holograms using a high-speed CMOS camera.

5. CONCLUSION

This paper has presented the thermo-mechanical characterization of surface-micromachined microheaters fabricated through PolyMUMPs, a three-layer polysilicon surface micromachining process used generally for MEMS applications. We have demonstrated that by using the unique feature of the lensless in-line digital holography technique, it is possible to obtain a quantitative map of thermal deformations on microstructures by applying the double-exposure method and without requiring aberration correction and focus-tracking. Thermal deformations determined using a lensless DH method match well with the results obtained from an analytical model. These results can be used to understand the thermal stress of the structure and thus, to ensure a reliable fabrication of the microheater. The results could also be utilized for evaluating the mechanical stability of the microstructures under high thermal stress.

ACKNOWLEDGEMENT

The authors would like to acknowledge the support received from the Ministry of Communication and Information Technology under Centre of Excellence in Nanoelectronics project. We also acknowledge the National MEMS Design Centre (NMDC) at Indian Institute of Science, Bangalore, for their support. We also thank the National Program on Micro and Smart Systems (NPMASS) for their support. We also acknowledge the support from the Department of Science and Technology.

REFERENCES

[1] Zhang R, Gu Y, Zhu D, Hao J and Tang Z 2002 Thermal measurement and analysis of micro hotplate array using *thermography Sensors Actuators* A **100** 144–52

[2] Liu W and Yang B 2007 Thermography techniques for integrated circuits and semi-conductor devices *Sensor Rev.* **27** 298–309

[3] Barton D L and Tangyunyong P 1996 Fluorescent microthermal imaging—theory and methodology for achieving high thermal resolution images *Microelectron. Eng.* **31** 271–9

[4] Csendes A, Szekely V and Rencz M 1996 Thermal mapping with liquid crystal method *Microelectron. Eng.* **31** 281–90

[5] Jorez S, Laconte J, Cornet A and Raskin J P 2005 Low-cost optical instrumentation for thermal characterization of MEMS *Meas. Sci. Technol.* **16** 1833–40

[6] Chen L C, Huang Y T and Fan K C 2007 A dynamic 3-D surface profilometer with nanoscale measurement resolution and MHz bandwidth for MEMS characterization *IEEE/ASME Trans. Mechatronics* **12** 299–307

[7] Wong C L and Wong W K 2007 In-plane motion characterization of MEMS resonators using stroboscopic scanning electron microscopy *Sensors Actuators* A **138** 167–78

[8] Volden T, Zimmermann M, Lange D, Brande O and Baltes H 2004 Dynamics of CMOS-based thermally actuated cantilever arrays for force microscopy *Sensors Actuators* A **115** 516–22

[9] Jayaraman B, Bhat N and Pratap R 2009 Thermal characterization of microheaters from the dynamic response *J. Micromech. Microeng.* **19** 085006

[10] Coppola G, Ferraro P, Iodice M, Nicola S D, Finizio A and Grilli S 2004 A digital holographic microscope for complete characterization of microelectromechanical systems *Meas. Sci. Technol.* **15** 529–39

[11] Coppola G, Striano V, Ferraro P, Nicola S D, Finizio A, Pierattini G and Maccagnani P 2007 A nondestructive dynamic characterization of a microheater through digital holographic microscopy *J. Microelectromech. Syst.* **16** 659–67

[12] Montfort F, Emery Y, Marquet F, Cuche E, Aspert N, Solanas E, Mehdaoui A, Ionescu A and Depeursinge C 2007 Process engineering and failure analysis of MEMS and MOEMS by digital holography microscopy (DHM) *Proc. SPIE* **6463** 63630G-1–7

[13] Xu L, Miao J and Asundi A 2000 Properties of digital holography based on in-line configuration *Opt. Eng.* **39** 3214–9

[14] Xu L, Guo P Z, Jianmin M and Asundi A 2005 Imaging analysis of digital holography *Opt. Exp.* **13** 2444–52

[15] Singh V R, Miao J, Wang Z, Hegde G M and Asundi A 2007 Dynamic characterization of MEMS diaphragm using time-averaged in-line digital holography *Opt. Commun.* **280** 285–90

[16] Koester D, Cowen A, Mahadevan R, Stonefield M and Hardy B 2003 *PolyMUMPs Design Handbook* (Berlin: MEMSCAP)

[17] Schnars U and Jüptner W 2002 Digital holography and numerical reconstruction of holograms *Meas. Sci. Technol.* **13** R85–101
[18] Ferraro P, De Nicola S, Finizio A, Coppola G, Grilli S, Magro C and Pierattini G 2003 Compensation of the inherent wave front curvature in digital holographic coherent microscopy for quantitative phase-contrast imaging *Appl. Opt.* **42** 1938–46
[19] Baroncini M, Placidi P, Cardinali G C and Scorzoni A 2004 Thermal characterization of a microheater for micromachined gas sensors *Sensors Actuators* A**115** 8–14
[20] Rossi C, Scheid E and Esteve D 1997 Theoretical and experimental study of silicon micromachined microheater with dielectric stacked membranes *Sensors Actuators* A**63** 183–9
[21] Han M H, Liang X and Tang Z A 2005 Size effect on heat transfer in micro gas sensors *Sensors Actuators* A**120** 397–402

List of Figures

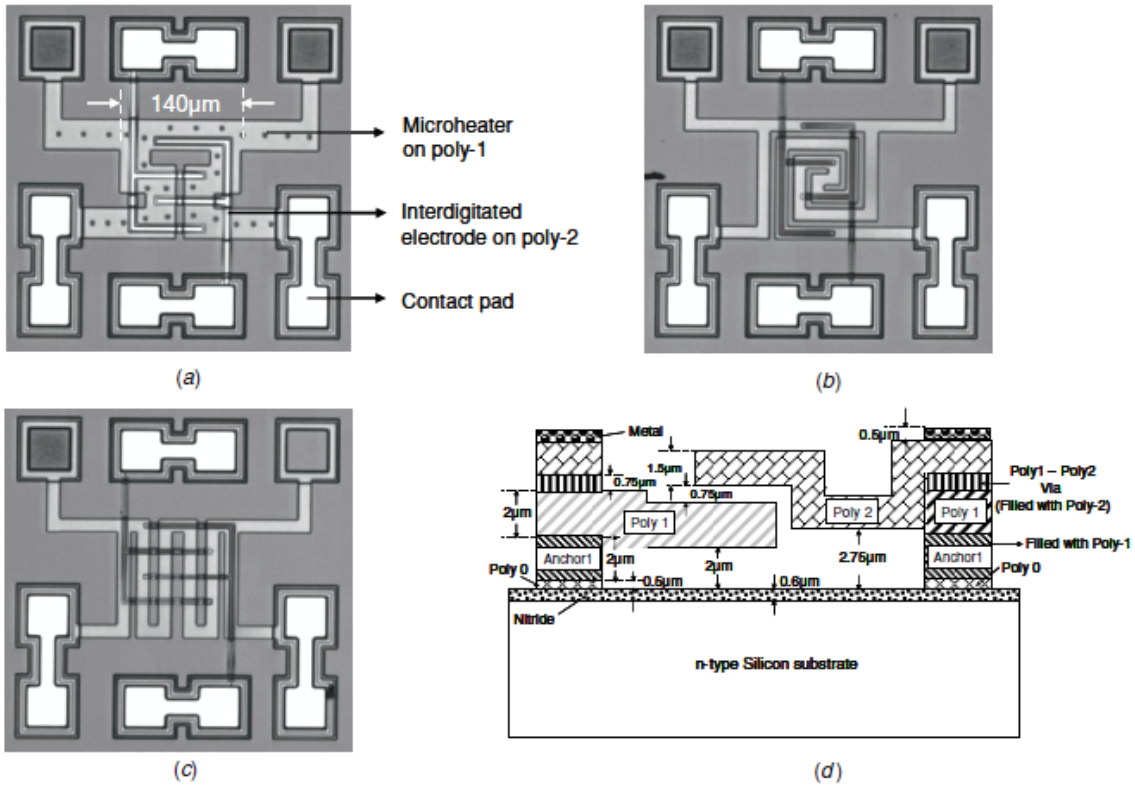
140μm
Microheater
on poly-1
Interdigitated
electrode on poly-2
Contact pad
(a)
(b)
(c)
Metal
0.5μm
1.5μm
0.75μm
0.75μm
2μm
Poly 1
Poly 2
Poly 1
Poly1 – Poly2
Via
(Filled with Poly-2)
Filled with Poly-1
Anchor1
2μm
2μm
2.75μm
Anchor1
Poly 0
0.6μm
0.6μm
Poly 0
Nitride
n-type Silicon substrate
(d)

Figure 1

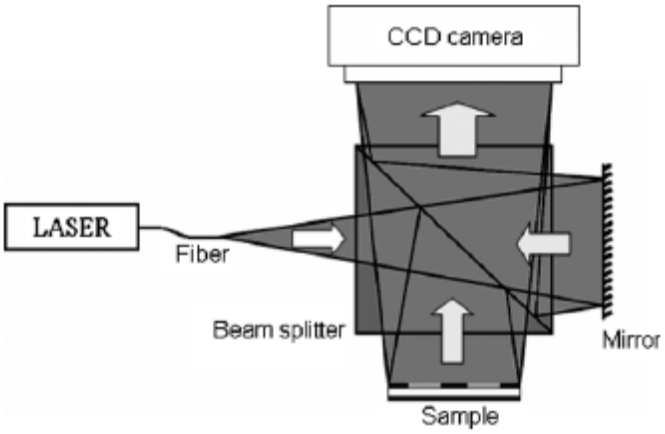

Figure 2

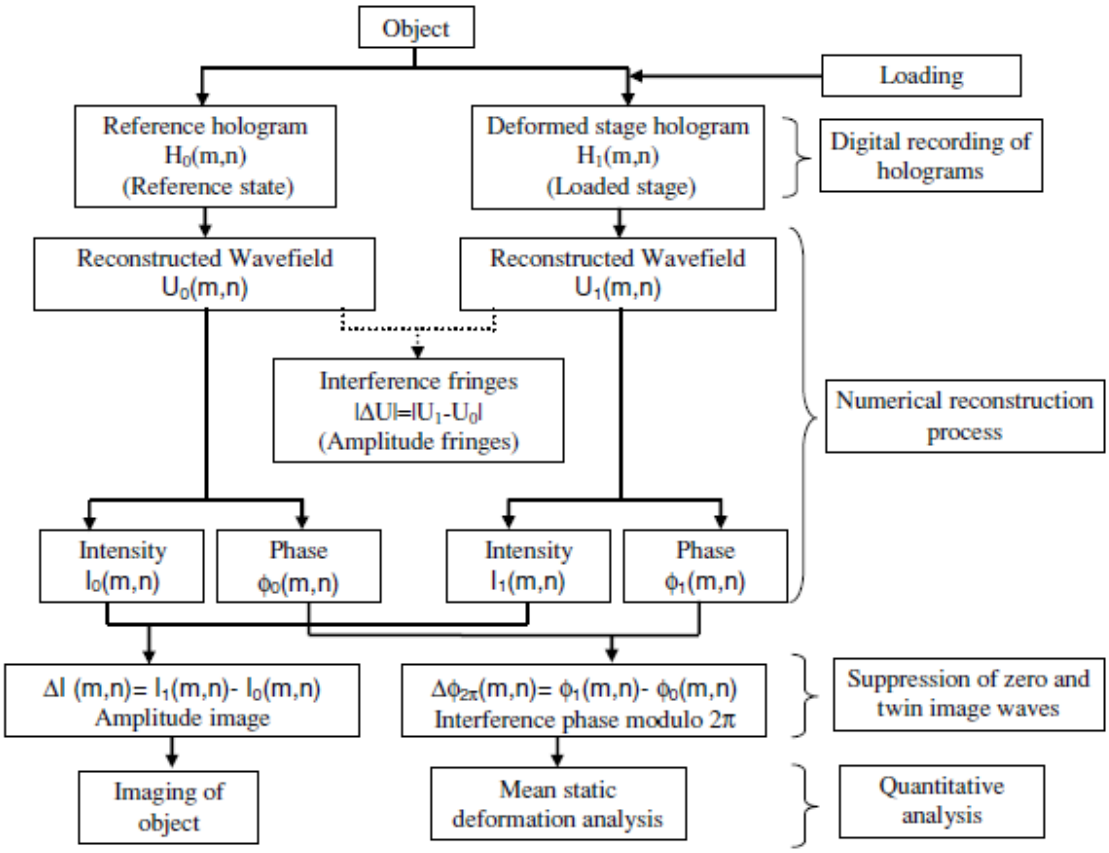
Object
Loading
Reference hologram
$H_0(m,n)$
(Reference state)
Deformed stage hologram
$H_1(m,n)$
(Loaded stage)
Digital recording of holograms
Reconstructed Wavefield
$U_0(m,n)$
Reconstructed Wavefield
$U_1(m,n)$
Interference fringes
$|\Delta U|=|U_1-U_0|$
(Amplitude fringes)
Numerical reconstruction process
Intensity
$I_0(m,n)$
Phase
$\phi_0(m,n)$
Intensity
$I_1(m,n)$
Phase
$\phi_1(m,n)$
$\Delta I\ (m,n)= I_1(m,n)- I_0(m,n)$
Amplitude image
$\Delta\phi_{2\pi}(m,n)= \phi_1(m,n)- \phi_0(m,n)$
Interference phase modulo 2π
Suppression of zero and twin image waves
Imaging of object
Mean static deformation analysis
Quantitative analysis

Figure 3

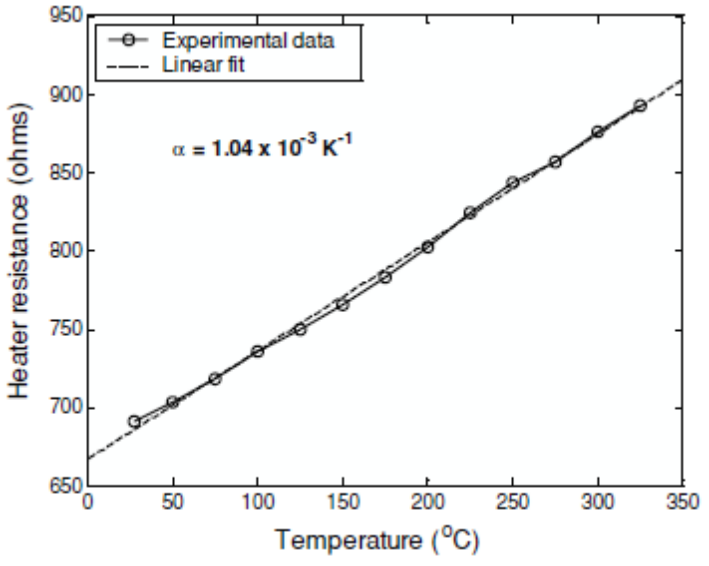
Experimental data
Linear fit
α = 1.04 x 10^-3 K^-1
Heater resistance (ohms)
Temperature (°C)
950
900
850
800
750
700
650
0
50
100
150
200
250
300
350

(*a*)

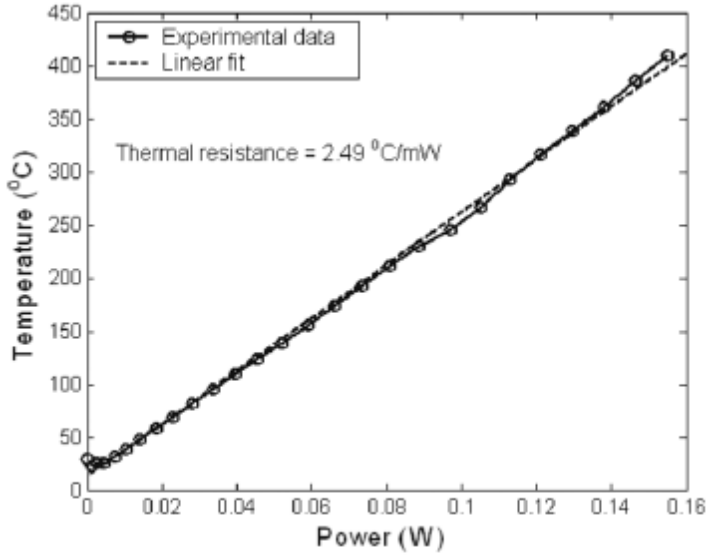
Experimental data
Linear fit
Thermal resistance = 2.49 °C/mW
Temperature (°C)
Power (W)
450
400
350
300
250
200
150
100
50
0
0
0.02
0.04
0.06
0.08
0.1
0.12
0.14
0.16

(*b*)

Figure 4

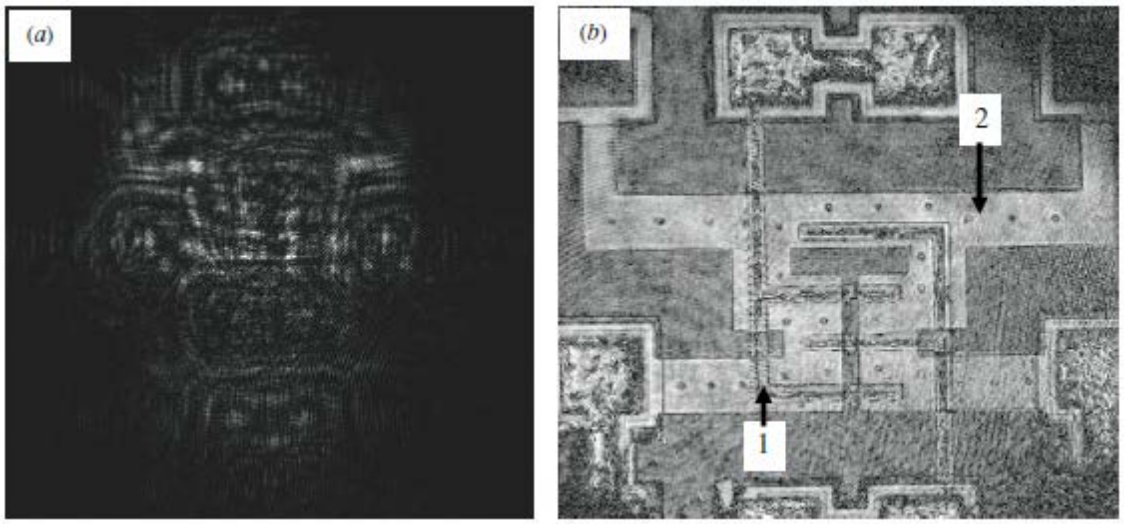

Figure 5

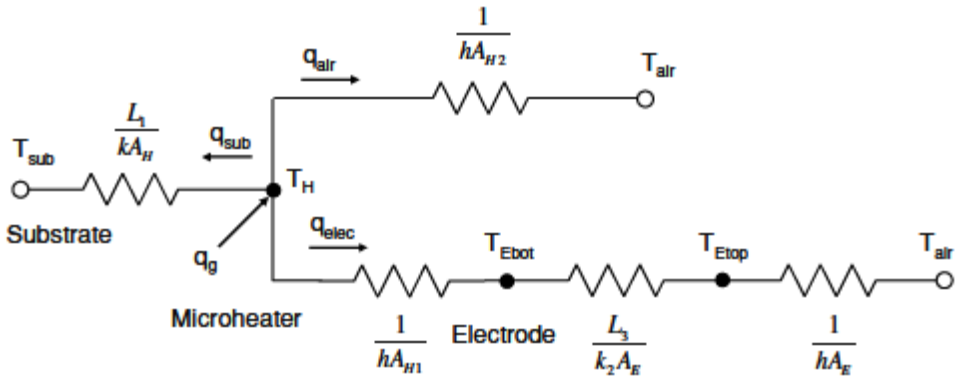
$\frac{1}{hA_{H2}}$
q_{air}
T_{air}
$\frac{L_1}{kA_H}$
q_{sub}
T_{sub}
T_H
Substrate
q_{elec}
q_g
T_{Ebot}
T_{Etop}
T_{air}
Microheater
$\frac{1}{hA_{H1}}$
Electrode
$\frac{L_3}{k_2 A_E}$
$\frac{1}{hA_E}$

Figure 6

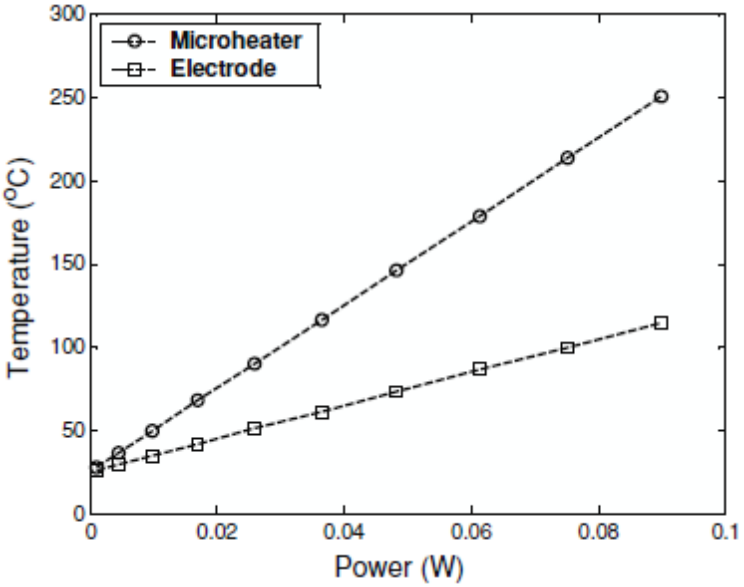
Microheater
Electrode
Temperature (°C)
Power (W)
300
250
200
150
100
50
0
0
0.02
0.04
0.06
0.08
0.1

Figure 7

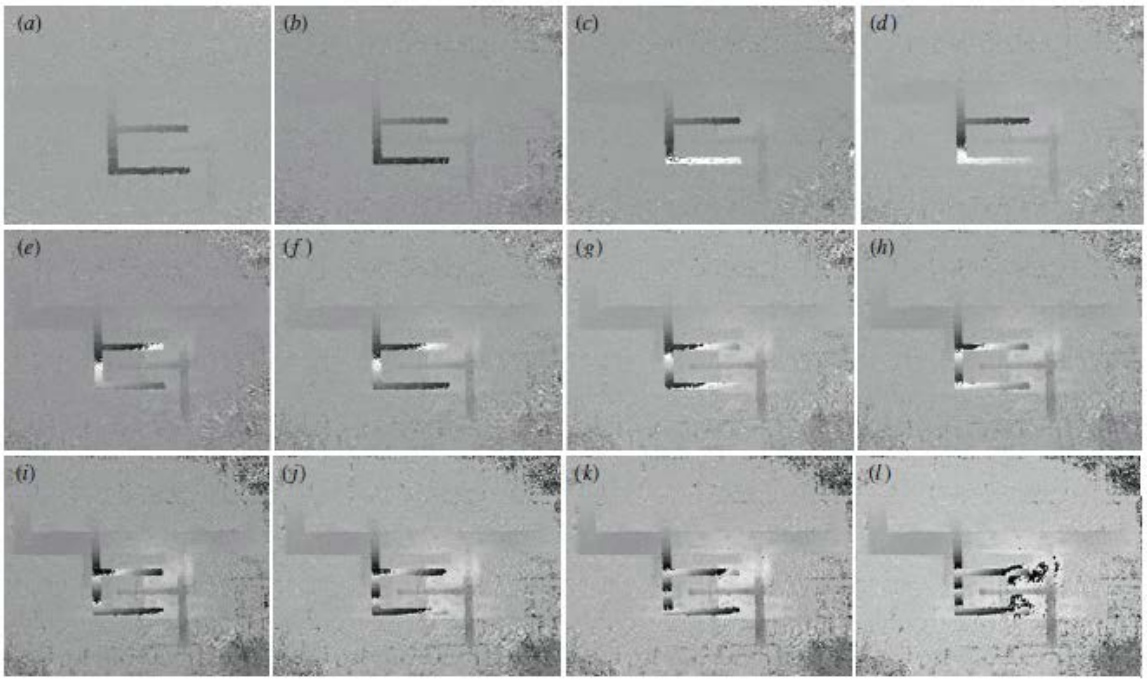

Figure 8

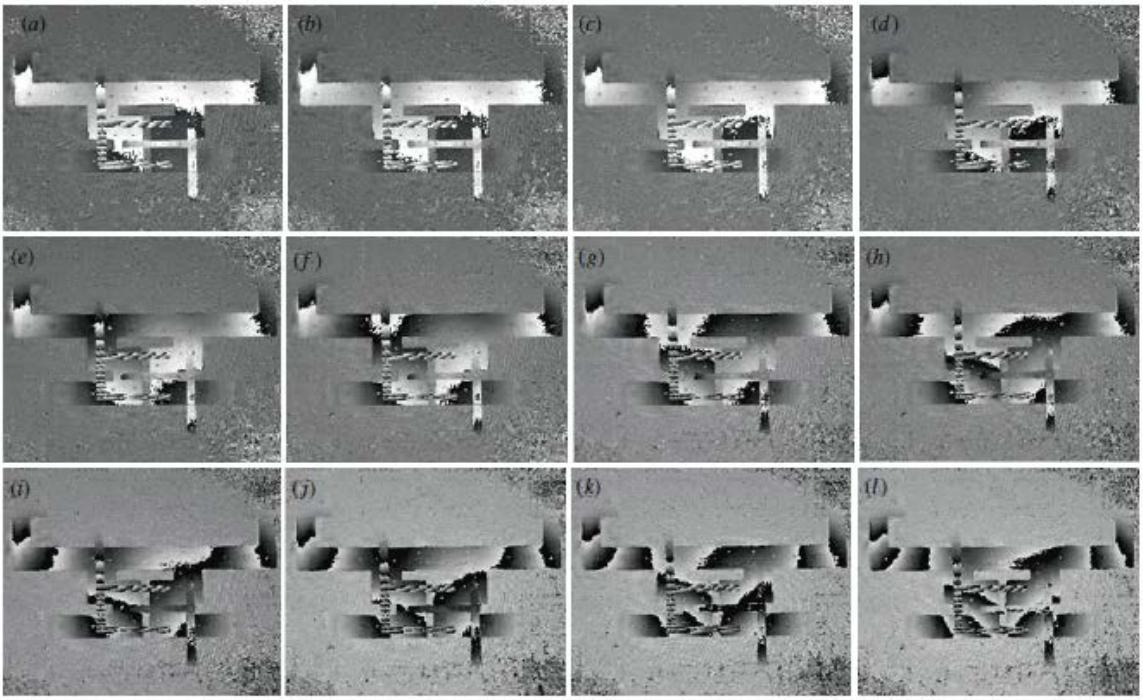

Figure 9

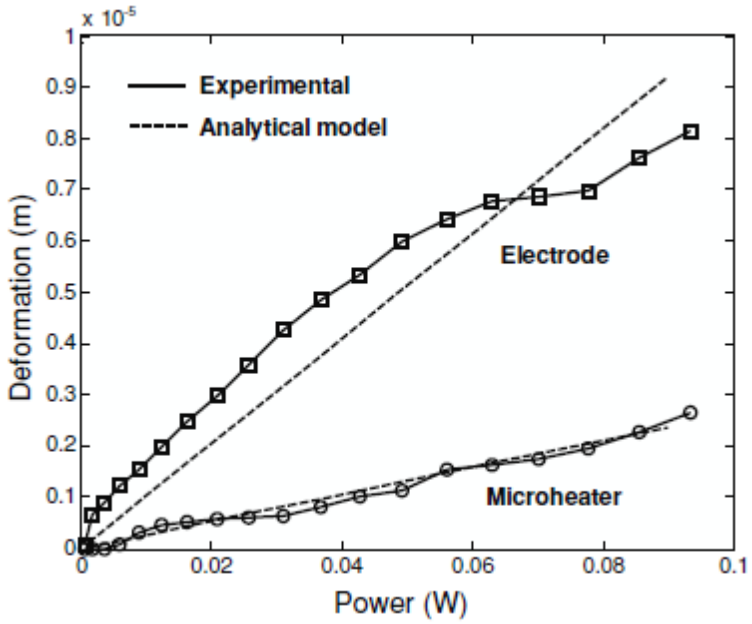
x 10^-5
Experimental
Analytical model
Electrode
Microheater
Deformation (m)
Power (W)
0
0.1
0.2
0.3
0.4
0.5
0.6
0.7
0.8
0.9
1
0.02
0.04
0.06
0.08
0.1

Figure 10